Published in final edited form as:
Nat Cell Biol. 2012 September ; 14(9): 911–923. doi:10.1038/ncb2566.

CDKL5 ensures excitatory synapse stability by reinforcing NGL-1-PSD95 interaction in the postsynaptic compartment and is impaired in patient iPSC-derived neurons

Sara Ricciardi[1], **Federica Ungaro**[1,#], **Melanie Hambrock**[2,#], **Nils Rademacher**[2], **Gilda Stefanelli**[1], **Dario Brambilla**[3], **Alessandro Sessa**[1], **Cinzia Magagnotti**[4], **Angela Bachi**[4], **Elisa Giarda**[5], **Chiara Verpelli**[6], **Charlotte Kilstrup-Nielsen**[5], **Carlo Sala**[6], **Vera M. Kalscheuer**[2,§,*], and **Vania Broccoli**[1,§,*]

[1] Stem Cells and Neurogenesis Unit, Division of Neuroscience, San Raffaele Scientific Institute, Milan, Italy

[2] Max Planck Institute for Molecular Genetics, Department of Human Molecular Genetics, Ihnestr. 73, D-14195, Berlin, Germany.

[3] Department of Human Physiology, University of Milan Medical School, Milan, Italy.

[4] Division of Genetics and Cell Biology, San Raffaele Scientific Institute, Milan, Italy

[5] Laboratory of Genetic and Epigenetic Control of Gene Expression, Department of Structural and Functional Biology, University of Insubria, 21052 Busto Arsizio, VA, Italy.

[6] Consiglio Nazionale delle Ricerche Neuroscience Institute, Milan, Italy.

Abstract

Mutations of the cyclin-dependent kinase like 5 (*CDKL5*) and netrin-G1 (*NTNG1*) genes cause a severe neurodevelopmental disorder with clinical features that are closely related to Rett syndrome (RTT), including intellectual disability, early onset intractable epilepsy and autism. We report here that CDKL5 is localized at excitatory synapses and contributes to correct dendritic spine structure and synapse activity. To exert this role CDKL5 binds and phosphorylates the cell adhesion molecule NGL-1. This phosphorylation event ensures a stable association between NGL-1 and PSD95. Accordingly, phospho-mutant NGL-1 is unable to induce synaptic contacts while its

[*]Correspondence should be addressed to: Vania Broccoli, Stem Cells and Neurogenesis Unit San Raffaele Scientific Institute Via Olgettina 58, 20132 Milan, Italy Tel: +39 02 26434616 broccoli.vania@hsr.it. Vera M. Kalscheuer, Max Planck Institute for Molecular Genetics Department Human Molecular Genetics, Ihnestr. 73, D-14195, Berlin, Germany. Tel: +49 30 84131293 kalscheu@molgen.mpg.de.
[#]Equally contributing authors
[§]Equally contributing senior authors

Author Contributions V.M.K. and N.R. initiated this study. S.R., M.H., N.R, V.M.K. and V.B. contributed to its conceptualization and V.M.K and V.B. directed it throughout, S.R. performed and analyzed neuronal experiments. F.U. generated iPSCs and characterized iPSC-derived neurons. M.H. performed and analyzed immunoprecipitations and Phos-Tag assays. M.H. and N.R. performed mutation search. G.S. was involved in mutagenesisexperiments. D.B. performed electrophysiological recordings. A.S. performed electroporation experiments. C.M. and A.B. performed 2D gel analysis. E.G. produced the CDKL5-specific antibody. C.V. and C.S. assisted with the preparation of primary neurons. C.K.-N. assisted with the in vitro phosphorylation assays. V.M.K., V.B., S.R., M.H. and N.R. interpreted the results. V.B., V.M.K. and S.R. wrote the manuscript.

Europe PMC Funders Author Manuscripts

phospho-mimetic form binds PSD95 more efficiently and partially rescues the CDKL5-specific spine defects. Interestingly, similar to rodent neurons, iPSC-derived neurons from patients with *CDKL5* mutations display aberrant dendritic spines, thus suggesting a common function of CDKL5 in mice and humans.

Europe PMC Funders Author Manuscripts

Introduction

Rett syndrome (RTT) is a severe neurodevelopmental disorder and is the most common genetic cause of intellectual disability in females[1,2]. The disorder is mainly caused by mutations in the methyl-CpG-binding protein 2 (*MECP2*) gene[3,4]. In addition to classical RTT, several atypical forms exist, including the Hanefeld variant, which is caused by mutations in the X-linked *CDKL5* gene. Patients present with early-onset intractable seizures starting before the age of 6 months and also show some typical symptoms of RTT although the clinical spectrum is heterogeneous[5-11]. This suggests that *CDKL5* mutations cause an early-onset neurodevelopmental disorder[12]. In a small number of patients *CDKL5* deletions have been reported[13-15]. These very likely caused loss-of CDKL5 function, similarly to what has been previously found in patients with a chromosome translocation that disrupted *CDKL5*[8,9] .*CDKL5* encodes a serine-threonine kinase whose catalytic domain shares homology with members of the cyclin-dependent kinase family and mitogen-activated protein kinases[16,17]. Interestingly, we showed that CDKL5 and MeCP2 are both induced at high levels during neuronal maturation and synaptogenesis. In addition, CDKL5 binds and phosphorylates MeCP2 *in vitro*[18]. Despite this molecular interplay, it is now well assessed that CDKL5 exerts its own functions, regardless of MeCP2[19-22]. However, the functional role of CDKL5 is presently unknown and thus, the question of how *CDKL5* mutations affect neuronal development and function and contribute to the pathophysiology of RTT remains to be answered.

Herein, we describe that *CDKL5* silencing leads to severe deficits in spine density and morphology. Notably, similar alterations were found in neurons established from patient fibroblast-derived pluripotent stem cells (iPSCs). Furthermore, we identified the netrin-G1 ligand (NGL-1, also known as LRRC4C) as a direct interactor and substrate of CDKL5. Importantly, NGL-1 phosphorylation strengthens the NGL-1-PSD95 interaction. Our findings demonstrate a novel role for CDKL5 in spine development and synapse morphogenesis.

Results

CDKL5 is enriched at the PSD of glutamatergic synapses

In the mouse, CDKL5 levels were highest in brain (Supplementary Fig. S1a,b). In postnatal day (P) 21 brain, CDKL5 immunoreactivity was evident in a punctate pattern in cell bodies as previously described (Fig. 1a)[20], and also along dendrites (Fig. 1b-c'). The expression of CDKL5 steadily increased during early postnatal brain development and, likewise, during maturation of *in vitro* cultured neurons (Supplementary Fig. S1c-f). Interestingly, some of the CDKL5 dendritic puncta localized to dendritic spines (Fig. 1c'). Subsequently, we investigated if CDKL5 is present at the postsynaptic density (PSD) and found that a large

number of CDKL5 puncta (61 ± 3%) co-localized with PSD95 in DIV15 neurons (Fig. 1d-f). Likewise, CDKL5 staining closely matched the pattern of other PSD markers (Fig. 1j). Consistent with a postsynaptic localization, CDKL5 immunolabeling was closely juxtaposed with presynaptic VGLUT1 (Fig. 1g). Triple staining for CDKL5, PSD95 and VGLUT1 confirmed CDKL5 localization at excitatory synapses (Fig. 1h, i). CDKL5 puncta coincided with the dot-like immunostaining of PSD95 and SHANK (Fig. 1k-m) and were apposed to VGLUT1 puncta also in brain (Fig. 1n-o'). To confirm the presence of CDKL5 at the PSD we performed a subcellular fractionation of mouse brain. CDKL5 was included in the synaptic fraction and in the entire PSD fraction (Fig. 1t). Further detergent solubilization of the synaptic plasma membrane fraction showed that CDKL5 is detectable in all PSD fractions, indicating its association with the PSD (Fig. 1t). Our studies also showed that CDKL5 co-localized marginally with inhibitory synaptic markers (Fig. 1p-s). Taken together, these findings indicate that CDKL5 is almost exclusively localized at excitatory synapses both *in vitro* and *in vivo*.

Loss of CDKL5 impairs spine structure and synaptic activity

To investigate the role of CDKL5 in dendritic spines, we silenced *CDKL5* in hippocampal neurons using two short-hairpin RNAs (sh-CDKL5#1, sh-CDKL5#2). In HEK293T cells both shRNAs down-regulated exogenous mouse CDKL5 levels by almost 80% (Supplementary Fig. S2a). Next, we infected DIV 7 hippocampal neurons with sh-CDKL5#1 and 7 days later observed a consistent reduction of CDKL5 (Supplementary Fig. S2b-h). Knock-down neurons showed a significant increase in protrusion density (Fig. 2a-i), the dendritic protrusions were significantly thinner compared to controls and showed a filopodia-like morphology (Fig. 2a-i). Notably, some of these thin filopodia-like spines were particularly branched and displayed an aberrant morphology (Fig. 2b'', b'''). Furthermore, the percentage of filopodia-like spines and thin headed spines increased, while the percentage of stubby and mushroom-shaped spines decreased (Fig. 2h, i). We obtained similar results for neurons infected at DIV 10 and analyzed at DIV 15 (data not shown). Conversely, we did not score any significant alteration in dendritic arborization (data not shown). These results indicate that CDKL5 is required for ensuring a correct number of well-shaped spines. Specificity was confirmed by the ability of a CDKL5 knock-down resistant form to rescue both, normal spine morphology and density (Supplementary Fig. S2i-o). The morphological alterations reported in CDKL5 silenced neurons were associated with a reduction in excitatory synapses and synaptophysin puncta in these neurons (Fig. 2j-s). To determine whether these alterations were accompanied with a reduction in overall synaptic activity, we examined spontaneous miniature excitatory post-synaptic currents (mEPSCs) in sh-CDKL5#1 transfected neurons. Consistent with the reduced excitatory synapse density, CDKL5 knock-down caused a significant decrease of mEPSCs (Fig. 2t-y) but had no significant effect on inhibitory synapse density and accordingly we did not detect any significant changes in miniature inhibitory postsynaptic currents (mIPSCs) (Supplementary Fig. S3). These results indicate that CDKL5 is necessary for correct dendritic spine structure and synapse activity.

Considering that CDKL5 is a kinase, we hypothesized that its phosphorylation activity is necessary for such function. To address this issue we used the CDKL5 K42R kinase-dead

form, which has a dominant-negative effect on wild-type CDKL5[16,19]. To analyze the effects of CDKL5K42R on spine density and morphology, we transfected DIV 7 hippocampal neurons with DsRed alone or combined with GFP-CDKL5K42R. Interestingly, GFP-CDKL5K42R immunolabeling was very similar to that of endogenous CDKL5 and there was a clear enrichment of the immunostaining in dendritic spines (Supplementary Fig. S2p-q'). Consistent with its dominant-negative action, neurons overexpressing GFP-CDKL5K42R displayed a significant higher number of thinner and longer dendritic protrusions and a corresponding loss of stubby and mushroom-shaped spines with respect to controls (Supplementary Fig. S2r-w). Since the phenotype discovered for the CDKL5K42R mutant was similar to the phenotype of CDKL5 knock-down neurons, it is conceivable that CDKL5 promotes spine formation through a mechanism that is dependent on its kinase activity.

Next, we sought to confirm the significance of our findings *in vivo* by electroporating E13.5 embryos *in utero* with a plasmid containing cassettes for independent expression of sh-CDKL5#1 and EGFP. Interestingly, at E18.5 CDKL5 down-regulated neurons showed a delay in radial migration. On the contrary, at P11 their relative location within the cerebral cortex was comparable to that of controls, thus indicating a transient delay in the definitive neuronal positioning (Fig. 3a, b and data not shown). Imaging of the GFP-labeled dendritic protrusions at P11, a crucial period of synaptogenesis, showed numerous protrusions with a large fraction having a well-defined head structure, characteristic of mature spines. Similar to the *in vitro* studies, sh-CDKL5#1 knock-down cortical pyramidal neurons showed a robust increase in protrusion density with dendritic protrusions significantly longer and dysmorphic (Fig. 3c-h). Next, we asked whether CDKL5 deficit might affect the number of functional excitatory synapses also *in vivo*. The density of VGLUT1 puncta identifying excitatory presynaptic buttons was significantly lower in sh-CDKL5#1 than in sh-Control pyramidal neurons (Fig. 3e, f, i), confirming that CDKL5 is crucial for dendritic spine morphogenesis and synaptic contact maintenance *in vivo*.

NGL cell adhesion molecules interact with CDKL5 at the PSD

Next, we set out to identify new CDKL5 interacting partners within dendritic spines. On the basis of our previous results showing that truncation of *NTNG1* caused atypical RTT with early-onset seizures[23], we considered the netrin-G1 receptor NGL-1 and the other members of the NGL family (NGL-2, -3, also known as LRRC4 and LRRC4B), which play a crucial role in early synapse formation and subsequent maturation[24,25] as a good starting point. Induction of NGL-netrin-G interaction promotes synapse formation[26,27]. In cells transfected with CDKL5-V5 and the intracellular domain of each of the NGLs, all three members were immunoprecipitated by the V5 antibody (Fig. 4a). In particular, CDKL5 binds specifically to a stretch of 5 amino acids located at the N-terminal side of the intracellular domain (Fig. 4b-d). Additionally, we screened other PSD enriched proteins that were directly or indirectly implicated in RTT-related disorders for CDKL5 interaction, but the results were negative (data not shown).

This prompted us to particularly characterize the association of CDKL5 with NGL-1. A co-clustering assay performed in cells co-transfected with GFP-CDKL5 and Myc-NGL-1,

indicated that these proteins form intracellular and surface co-clusters (Fig. 4e-i). In fact, while CDKL5 localized in the cytoplasm when transfected alone, co-expression with NGL-1 resulted in CDKL5 translocation to the cell membrane and exact overlapping with NGL-1 (Fig. 4g-h). Further tests in a more physiological context showed that in hippocampal neurons both proteins co-localized precisely at dendritic spines (Fig. 4j-j'''). Similarly, Myc-NGL-1 also highly co-localized with endogenous CDKL5 (Fig. 4k-m). Next, the interaction of the proteins was assessed using P4 synaptosome brain extracts. Indeed, NGL-1 was co-immunoprecipitated by the CDKL5 antibody (Fig. 4n), indicating that NGL-1 assembles in the CDKL5 complex *in vivo*. Notably, both proteins even directly interact as ascertained by a pull-down assay (Fig. 4o).

These data prompted us to speculate that CDKL5 might phosphorylate NGL-1. At first, we analyzed whether NGL-1 is phosphorylated in mouse brain by performing 2D-SDS-PAGE from P10 extracts (Fig. 5a). NGL-1 specific staining was resolved in two protein spots. Since addition of the phosphatase CIP robustly reduced the intensity of only spot 2, while spot 1 increased its relative signal, we concluded that spot 2 did represent the phosphorylated form of NGL-1 (Fig. 5a).

Subsequently, we subjected the entire or parts of the NGL-1 intracellular domain to Phos-Tag staining. Interestingly, only the entire and the C2 N-terminal part produced an additional upper band that presents a putatively phosphorylated protein as confirmed by its loss after CIP treatment (Fig. 5b). These results indicate that NGL-1 is present with a mono-phosphorylated form both, *in vitro* and *in vivo*.

CDKL5 phosphorylates NGL-1 at S631

NGLs' C2 N-terminal domain has several amino acids conserved between the family members, including S600, S620 and S631. We mutated these serines into non-phosphorylable alanines and repeated the Phos-Tag assays. Importantly, our results identified NGL-1 S631, but not S600 or S620, to be phosphorylated (Fig. 5c). To obtain direct evidence of the CDKL5 ability to induce NGL-1 protein phosphorylation, the C-terminal half of NGL-1 (aa 550-640) was purified and used for *in vitro* kinase assays. Interestingly, NGL-1 is readily phosphorylated in the presence of CDKL5. In contrast, mutant S631A was not phosphorylated by CDKL5 (Fig. 5d). The catalytic activity of CDKL5 has been reported to be involved in its auto-phosphorylation *in vitro*[16,18]. Consistent with this, we observed auto-phosphorylation when CDKL5 was added (Fig. 5d).

To address if the NGL-1 S631A mutant could be co-immunoprecipitated by CDKL5, we analyzed their interaction. Noteworthy, GFP-CDKL5 failed to co-immunoprecipitate NGL-1 S631A, thus suggesting the relevance of the phoshorylation for reinforcing the interaction (Fig. 5e). To gain further support, we analyzed the NGL-1 binding ability of various CDKL5 deletion mutants. Notably, none of the mutants lacking the kinase domain or its activity were able to immunoprecipitate NGL-1 (Supplementary Fig. S4) suggesting that the kinase domain and CDKL5 auto-phosphorylation are necessary for the stable interaction of CDKL5 with NGL-1.

We next investigated the phosphorylation level of NGL-1 in a fibroblast cell line derived from a female patient who carried a X;7 chromosome translocation that trunctated *CDKL5* and due to inactivation of the normal X-chromosome lacked functional CDKL5[8]. Importantly, the patient cells when compared to normal control fibroblasts which express endogenous CDKL5 exhibited reduced levels of the NGL-1 phosphorylated form with respect to the total amount of the protein (Fig. 5f). Thus, these data suggest that the CDKL5/NGL-1 protein interaction is conserved in human cells and that also in fibroblasts NGL-1 is phosphorylated by CDKL5. Along the same line, an increment of the NGL-1 phosphorylated form was detected when CDKL5 was overexpressed in the patient fibroblasts. This effect was not seen in normal control fibroblasts, suggesting that in these cells NGL-1 S631 phosphorylation was already saturated by endogenous CDKL5 (Fig. 5g).

NGL-1 binding to PSD95 is sustained by CDKL5 phosphorylation on S631

NGLs show a conserved C-terminal PDZ binding domain (VQETQI), which specifically binds to PSD95[27] that plays a significant role in learning and memory[29]. NGL-1 spine inducing capability is promoted by targeting PSD95 to new forming dendritic protrusions[27]. Given that CDKL5 interacts directly with NGL-1, we wondered whether CDKL5 might influence the interaction of these proteins. To test this, we performed a co-immunoprecipitation assay in cortical neurons infected at DIV 7 with sh-CDKL5#1. Seven days later, NGL-1 was immunoprecipitated and the amount of PSD95 in the complex was determined. Remarkably, we observed a robust reduction of the NGL-1-PSD95 interaction in CDKL5 knock-down neurons (Fig. 6a). These results indicate that CDKL5 functions in promoting and/or maintaining the NGL-1-PSD95 protein association.

NGL-1 phosphorylated residue S631 is very close to the terminal PDZ binding domain and therefore located at a convenient site for regulating NGL-1-PSD95 interaction. To test this, we transfected cells with either NGL-1 or its S631A phospho-mutant in combination with GFP-PSD95, immunoprecipitated the lysates for Myc-NGL-1 and measured the amount of associated PSD95. Indeed, the phospho-mutant showed reduced association with PSD95 (Fig. 6a). Next, we tested the ability of the mutant to promote synaptogenesis in hippocampal neurons. Notably, dendritic protrusions were reduced in numbers and showed a significantly elongated morphology (Fig. 6b, c). These alterations are both qualitatively and quantitatively similar to the phenotype observed in CDKL5 down-regulated neurons. Therefore, it is plausible that the NGL-1 S631A mutant acts through a dominant-negative effect on endogenous NGL-1 and its ability to associate with PSD95.

To further strengthen this assumption, the phospho-mimetic NGL-1 mutant S631E was challenged in similar experiments. In particular, this mutant associated better with PSD95 although it was not able to significantly increase spine formation upon overexpression (Fig. 6b, c). Despite that, when expressed in CDKL5 knock-down neurons, the mutant was capable to restore nearly correct length and morphology of dendritic spines, but not their numbers (Fig. 6f, g). Conversely, both phospho-mutants retained the ability to induce pre-synaptic terminals similar to the native NGL-1 when expressed by heterologous cells co-cultured with primary neurons (Supplementary Fig. S5)[27]. These findings are consistent with the NGL-1 extracellular domain being the main molecular player of this activity.

In overall, these data indicate that CDKL5 is of critical relevance for the maintenance of synaptic contacts, which is mainly achieved by regulating the NGL-1 phosphorylated state and, thereby, its ability to bind PSD95 and stabilize their association.

Patient-specific alterations in iPSC-derived neurons

iPSC technology offers the possibility to model *in vitro* neurodevelopmental disorders by providing access to human neurons. Therefore, we set out to establish iPSC lines from two female patients diagnosed with atypical RTT caused by *CDKL5* pathogenic mutations (R59X, L220P) and whose primary fibroblasts were already characterized[20,30]. Fibroblasts were infected with OCT4, SOX2 and KLF4-expressing retroviruses and cultured in the presence of SR and FGF2. After 6-8 weeks, the iPSC-like clones expressed pluripotency markers and showed silencing of the retroviral exogenous genes (Fig. 7a and Supplementary Fig. S6a,b, Fig. S7a,b). Pluripotent properties were also ascertained by testing the capability to differentiate into cells of the endoderm ($SOX17^+$), mesoderm (SMA^+) and neuroectoderm ($TuJ1^+$) germ layers *in vitro* and the potential to generate teratomas (Supplementary Fig. S6c,d). Further, correct chromosomal content was ascertained by karyotyping (Supplementary Fig. S7c).

Increasing evidence shows that female iPSCs may or may not retain the inactivated X-chromosome status of the original fibroblasts[31-33]. Indeed, only iPSCs exclusively expressing the mutant *CDKL5* allele will represent a coherent model of disease-affected cells. Thus, we only investigated those clones in which inherent X-chromosome inactivation was revealed by H3K27me3 nuclear staining (Fig. 7a) and selected only cell lines, which showed expression of either the mutant or the normal *CDKL5* allele for further analysis. This approach allowed the generation of both, pathogenic and healthy iPSCs from the same individual providing stringent control cells for comparative analyses. A list of the cell lines used for each experiment is detailed in Supplementary Table 1.

Undifferentiated mutant and control iPSC clones did not show any evident difference (data not shown). We then induced their differentiation into neurons through generation of neural-rosette intermediate neural progenitors and their subsequent differentiation for 55-60 days[34]. In these conditions, neuronal cultures developed a highly intricate neuronal network highly enriched in forebrain committed glutamatergic neurons (Fig. 7b-h). Interestingly, CDKL5 expression was found to strongly increase following neuronal differentiation (Fig. 8a). In particular, CDKL5 was found enriched in dendritic spines in well-matured neurons (Fig. 8b). These findings establish iPSC-derived neurons as an adequate *in vitro* model to study CDKL5-dependent biological mechanisms. Absence of CDKL5 did not impair the rate of neuronal differentiation or morphology (Fig. 8c-g). Interestingly, a significantly reduced number of synaptic contacts, indicated by the number of VGLUT1 and PSD95 puncta was detected in the mutants (Fig. 8h-m). To highlight spine morphology, neurons were infected with a constitutively expressing GFP lentivirus at low multiplicity. This staining permitted to visualize frequent abnormalities in the overall spine structure of mutant neurons (Fig. 8n-r). In particular, many of these altered spines did not present an evident pre-synaptic terminal (Fig. 8p, q). These results are well in line with those obtained for CDKL5 silenced mouse

neurons and suggest a conserved role of this protein in neuronal structure homeostasis and activity.

Discussion

In this study, we revealed how loss of CDKL5, the molecule responsible for the Hanefeld variant of RTT and early-onset intractable encephalopathy, impacts neuronal function. Our first observations indicate that CDKL5 mainly localizes to dendritic spines where it is juxtaposed to the PSD. Interestingly, CDKL5 was found in the human PSD[35] (www.genes2cognition.org/HUMAN-PSD), suggesting that its localization at the synaptic PSD is evolutionary conserved. Our data provide evidence that CDKL5 is necessary for correct genesis and maintenance of dendritic spines and for synapse formation. Indeed, knocking down CDKL5 significantly decreases the density and length of dendritic spines both, *in vitro* and *in vivo*.

In line with the compromised development of spines, CDKL5 down-regulated neurons exhibit abnormal mEPSCs. Thus, our results reveal that CDKL5 is a key-limiting factor in regulating glutamatergic synapse formation and suggest that changes in excitatory synaptic strength might be responsible, at least in part, for the neurodevelopmental symptoms associated with its deficiency.

We identified CDKL5 as an interactor of NGLs, which are synaptic cell adhesion molecules (CAMs) that exert a pervasive role in synapse homeostasis[24,27,36-38]. Very intriguingly, we havepreviously found that *NTNG1*, which encodes the specific NGL-1 partner netrin-G1, was disrupted by a chromosome translocation in a patient with atypical RTT[23]. It is then highly plausible that CDKL5 and NGL-1 might work, at least in part, in a common pathway thus providing a molecular framework explaining the similar neuropathological outcome of *NTNG1* and *CDKL5* mutations.

Our findings prompted us to search for pathogenic mutations in *NGL-1, -2* in patients with atypical RTT. No likely pathogenic changes were detected in these genes, suggesting that they are not a major contributor (data not shown). Despite we did not detect *NGL-1, -2* mutations, other groups reported deletions including *NTNG1* in patients presented with intellectual disability and seizures[39], *NTNG1* missense mutations in autism[40], and the association of *NTNG1* non-coding single nucleotide polymorphisms with schizophrenia[41].

We provide evidence that CDKL5 phosphorylates NGL-1 on a unique serine, which is very close to the PDZ binding domain that interacts with PSD95. This phosphorylation can also be extracted from a phospho-proteomic survey of mouse tissues[28]. To date, little evidence exists showing that the activity of synaptic CAMs is controlled by post-translational mechanisms. The discovery of a regulated phosphorylation process in NGL-1 opens the exciting possibility that the activity of other CAMs can be controlled by their phosphorylation state.

We demonstrated that CDKL5 is able to phosphorylate NGL-1 at S631 both, *in vitro* and in mouse brain. Importantly, the same results were obtained for human cells. In fact, CDKL5 negative patient fibroblasts exhibited reduced NGL-1 phosphorylation when compared to

control cells. Since NGL-1 phosphorylation was not completely absent, it is plausible to assume that other kinases substitute for CDKL5 in these cells. To overcome the limitations of using skin fibroblasts, we generated iPSC-derived neurons from two female patients with atypical RTT. Interestingly, in these neurons we detected a loss of synaptic contacts together with an increased number of aberrant dendritic spines indicating that they represent a reliable system for studying CDKL5 function.

We showed that CDKL5-mediated phosphorylation of NGL-1 is necessary to ensure stable binding to PSD95. This mechanism resembles the phosphorylation dynamics of ion channels that mediate changes in the interaction with PSD95[42,43]. Furthermore, phosphorylation of serine at position -9 outside the PDZ-binding domain in ephrin B ligands is required for the stable interaction with GRIP at the PSD and ensures correct synaptic activity[44]. These results mirror our findings and highlight a new aspect of fine-tuning protein-protein interaction by serine phosphorylation.

Interestingly, overexpression of a NGL-1 non-phosphorylable mutant leads to significant elongation of dendritic protrusions. This phenotype closely resembles the defects observed in CDKL5 silenced neurons, suggesting that the mutant could act in a dominant-negative manner leading to disruption of the NGL-1-PSD95 interaction. Thus, these data indicate that synaptic strength and stability can be modified by altering the ratio between phosphorylated and unphosphorylated NGL-1 and, possibly, its homologs.

Our results are consistent with a model in which loss of CDKL5 elicits spine length and synaptic strength by regulating NGL-1-PSD95 interaction. On the other hand, CDKL5 interacts with Rac1[21], which participates in stabilizing the actin cytoskeleton. Therefore, it is possible that Rac1 activity is altered by CDKL5 deletion. This is particularly relevant given that actin filament dynamics within the spines control their morphology and stability[45]. Thus, we cannot exclude that some aspects of the alterations described in this study can be ascribed to defects in such mechanisms. In agreement with this assumption, rescue of CDKL5-dependent spine deficits by a phospho-mimetic NGL-1 mutant is incomplete suggesting that other mechanisms are dysregulated by CDKL5 impairment.

In conclusion, we demonstrate that loss of CDKL5 severely affects spine morphology and reduces functional synaptic contacts impairing neuronal activity.

We propose a model in which CDKL5-dependent phosphorylation on S631 controls the association of NGL-1 with the postsynaptic molecular hub PSD95. In light of these findings, we provide novel mechanistic insights into how *CDKL5* mutations can impact on neuronal function in atypical forms of RTT and other CDKL5-related neurodevelopmental disorders.

Methods

Plasmids and constructs

pEGFP-hCDKL5, pEGFP-hCDKL5 ΔN, pEGFP-hCDKL5 Δ525, pEGFP-hCDKL5 Δ781, pEGFP-hCDKL5 Δ832, pEGFP-hCDKL5 832-1030 and pEGFP-hCDKL5 K42R were described previously[16,19].

For cloning of the NGL-1 cytoplasmic region or its C1 and C2 fragments we used the pEGFP-C2 vector (Clontech) double-digested with *Eco*RI und *Sal*I restriction enzymes (New England Biolabs) and PCR products generated using genomic DNA as template with the following primer pairs: NGL-1 pEGFP EcoRIfor TAGAATTCAAGATGAGGAAGCAGCACC, NGL-1 pEGFP SalIrev TAGTCGACTTAGATTTGAGTCTCTT; NGL-1 C1 pEGFP EcoRIfor TAGAATTCAAGATGAGGAAGCAGCACC and NGL-1 C1 pEGFP SalIrev TAGTCGACTTACATGGGTGTGTCTCCCG; NGL-1 C2 pEGFP EcoRIfor TAGAATTCGAAAGCCACCTGCCCATGC and NGL-1 C2 pEGFP SalIrev TAGTCGACTTAGATTTGAGTCTCTT.

The lentiviral knock-down constructs were generated by cloning oligoduplexes into pLentiLox 3.7 (pLL 3.7) according to the protocol published online by Science gateway (http://www.sciencegateway.org/protocols/lentivirus/cloning.htm). The sh-CDKL5#1 construct targets the region AGGAGCCTATGGAGTTGTA, the sh-CDKL5#2 construct is directed against the target region TGATAGCAGTTCTGGTACA and the sh-control construct is directed against Renilla luciferase and targets the region GGCCTTTCACTACTCCTAC. pMyc-hNGL1 was a gift from E. Kim (Korea Advanced Institute of Science and Technology, Daejeon, Republic of Korea). pEGFP-PSD95 was a gift from L. Muzio (San Raffaele Scientific Institute, Milan, Italy). pMXOCT4, pMXSOX2, pMXKLF4 were a gift by S.Yamanaka (Gladstone Institute, University of California). The S631A, S631E and S600A derivatives were generated by site-directed mutagenesis using the Quick change II site-directed Mutagenesis Kit (Stratagene). pCAGGS-hNGL1-iresEGFP and pCAGGS-NGL1-S631A-iresEGFP were generated by PCR and cloned into the *Eco*RI site of pCAGGS-iresEGFP. Recombinant hNGL1 (550-640AA) and hNGL1 (550-640AA) S631A were produced from the pTYB1-NGL1 and pTYB1-NGL1-S631A constructs cloned by PCR into the *Nde*I and *Xho*I sites of pTYB1 (New England Biolabs) generating a chitin-binding fusion protein. All PCR-generated constructs were verified by sequencing.

Cell culture and transfection

HEK293T, COS-7 and fibroblast cells were cultured in Dulbecco's modified Eagle's medium (Invitrogen) supplemented with 1% penicillin/streptomycin (Sigma Aldrich, St Louis, MO), 2 mM glutamine (Sigma Aldrich) and 10% fetal bovine serum (Invitrogen) at 37°C with 5% CO_2. Transient DNA transfections were carried out using Lipofectamine 2000 (Invitrogen) according to the manufacturer's recommendations or the calcium phosphate precipitation method.

Primary hippocampal and cortical cultures

Primary neuronal cultures were prepared as described previously[20].

Mixed-culture assay

Mixed-culture assay was carried as described previously[40].

Retrovirus infection, iPSCs derivation and differentiation

Female CDKL5 fibroblasts derived from two patients' specific dermal biopsies explants were kindly provided by Thierry Bienvenu's group (Cochin Institute, Paris, France). They were maintained *in vitro* for two passages before infection with three retrovirus cocktails (OCT4, SOX2 and KLF4). 2.5×10^5 fibroblasts were infected with the retroviral cocktail for each reprogramming experiment; two days after infection, fibroblasts were plated on mitotically inactivated murine embryonic fibroblasts (MEF) layer on Matrigel™ (BD) coated dishes. After 6-8 weeks in culture in hES medium (DMEM F12, 1 mM Sodium Pyruvate, 1X NEA, 20 μM β-Mercaptoethanol, 20% Knockout Serum Replacements, 10 ng/ml FGF2; Invitrogen), the first hiPSC clones appeared and were manually picked. Thus, they were cultured and expanded in hESCs conditions on MEF feeders layer on Matrigel™ (BD) coated dishes. For differentiation into the three germ layers, hiPSC colonies were incubated in 1 mg/ml collagenase IV (Invitrogen) for 1 hour at 37°C, detached and collected. They were cultured in suspension for 5 days in EB medium (hES without FGF2) and plated on 1 mg/ml gelatine (Sigma) coated dishes for up to 20 days in 20% Fetal Bovine Serum (Invitrogen). For neuronal differentiation, EBs were cultured for 5 days in suspension in EB medium, then plated and cultured on Matrigel™ coated dishes in N2/FGF medium (DMEM F12, 1X N2 supplement, 20 ng/ml FGF2; Invitrogen) for 3-5 days. After 3-5 days, appearing rosette-like structures were picked and manually disaggregated; then, they were plated on a layer of glial cells derived from E14.5 mouse cortices in N2/FGF medium for 1 day and then cultured in B27/AA medium (Neurobasal medium, 1X B27 supplement; Invitrogen; 20 μM Ascorbic Acid; Fluka; 20 ng/ml BDNF; Peprotech) for 55-60 days. For spine length analysis, manually disaggregated rosette structures were plated on Matrigel™ for 1 day, then infected by lentivirus carrying GFP reporter (pLL3.7-GFP) and maintained in culture for 3 days. Infected cells were manually detached and plated again on mouse astrocyte layers. They were cultured on astrocytes for 55-60 days in B27/AA medium and then fixed for further analysis.

Immunofluorescence

Hippocampal neurons were fixed for 10 min in methanol (-20°C) or 4% paraformaldehyde for 20 min at room temperature. Immunofluorescence was performed as described previously[20]. The following primary antibodies were used: immunopurified rabbit polyclonal anti-CDKL5 (1:5)[19], mouse monoclonal anti-NGL1 (clone N49A/21; 1:500, Neuromab), mouse monoclonal anti-GFP (clone 3E6; 1:500, Invitrogen), chicken polyclonal anti-GFP (1:2,000, Invitrogen), mouse monoclonal anti-MAP2 (clone MT-01; 1:500, Immunological Science), mouse monoclonal anti-PSD95 (clone K28/43; 1:200, Neuromab), mouse monoclonal anti-synaptophysin (clone 7.2; 1:1,000, Synaptic System), mouse monoclonal anti-VGLUT1 (clone 317G6; 1:500, Synaptic System), guinea-pig polyclonal anti-VGLUT1 (1:500, Synaptic System), mouse monoclonal anti-Pan-Shank (clone N23B/49; 1:400, Neuromab), mouse monoclonal anti-NR2A (clone N327/95; 1:400, Neuromab); mouse monoclonal anti-OCT4 (1:500, Santa Cruz Biology), rabbit polyclonal anti-SOX2 (1:200, Abcam), mouse monoclonal anti-TRA-1-60 (clone TRA-1-60; 1:200, Millipore), rabbit polyclonal anti-NANOG (1:200, Abcam), rabbit polyclonal anti-Tuj1 (1:200, Covance). Alexa 488, 594 and 647 anti-chicken, anti-mouse, anti-rabbit and anti-guinea-pig IgG secondary antibodies (1:500, Molecular Probes) were used for detection. For

alkaline phosphatase staining, cells were fixed in 2% paraformaldehyde for 10 min, washed with PBS and incubated in 0.1% Triton X-100 NTMT (100 mM NaCl, 100 mM Tris-HCl, 100 mM Tris, 50 mM $MgCl_2$), supplemented with BCIP and NBT (Roche) for 10 min. Bright field images were detected by a upright Leica microscope.

RNA Extraction and qRT-PCR

All RNA samples were extracted with RNeasy Micro Kit (Quiagen) from 1 to 5×10^6 cells, according to the manufacturer's instruction. RNA strands were retro-transcribed using the Transcriptor High Fidelity cDNA Synthesis Kit (Roche) and cDNAs were amplified by Amplibiotherm DNA polymerase (Fisher Molecular Biology). For qRT-PCR, SsoFast EvaGreen Supermix™ (BioRad) was used according to the manufacturer's instruction.

Immunoprecipitation and Western blot

Immunoprecipitation on cell transiently co-transfected using the calcium phosphate precipitation method or Lipofectamine 2000 (Invitrogen) and Western blot were performed as described previously[20]. The following primary antibodies were used: mouse monoclonal anti-GFP (clones 7.1 and 13.1; 1:1,000, Roche Diagnostics), mouse monoclonal anti-PSD95 (clone K28/43; 1:1,000, Neuromab), mouse monoclonal anti-synaptophysin (clone 7.2; 1:5,000, Synaptic System), mouse monoclonal anti-GAPDH (clone 6C5; 1:5,000, Millipore), rabbit polyclonal anti-CDKL5 (1:1,000, Sigma), goat polyclonal anti-GFP-HRP (1:5,000, Abcam), mouse monoclonal anti-V5 (1:1,000, Invitrogen), and mouse monoclonal anti-tubulin (clone DM1A; 1:15,000, Abcam). Prior to CIP treatment of immunoprecipitations and phosphate-affinity PAGE, cells were collected and lyzed in 50 mM Tris-HCl, pH 8.0, 150 mM NaCl, 1% NP-40 supplemented with EDTA-free protease inhibitors (Roche). For CIP treatment beads were resuspended in 20 µl H_2O, splitted and each sample was supplied with 3 µl buffer NEB3 (New England Biolabs). Then, 10 U CIP (New England Biolabs) were added to the respective samples. All samples were incubated for 1 h at 37°C prior to western blot analysis.

Phosphate-affinity polyacrylamide gel electrophoresis

The dinuclear metal complex Mn2+-Phos-Tag™ acts as a phosphate-binding tag molecule and allows separation of phosphorylated and non-phosphorylated proteins in SDS-PAGE by mobility shift detection.Here we used 10% SDS-gels with 50µM Phos-Tag™ acrylamide (Nard Institute, Ltd) and 100 µM $MnCl_2$ (Sigma) according to the manufacturer's recommendations.

2D-PAGE

Mouse brains were manually broken up using a dounce homogenizer and then resuspended in 500 µl of lysis buffer (5 M urea, 2 M thiourea, 2% CHAPS w/v, 2% Zwittergent v/v, protease and phosphatase inhibitors). The lysates were centrifuged at 16,000 *g* for 30 minutes at 15°C and stored at -80°C. The recovered supernatant was analyzed to determine total protein concentration using BioRad protein assay and BSA as standard. For 2D electrophoresis, 300 µg total protein were loaded on each gel and each sample was run in triplicates. Prior to the first dimension of isoelectrofocusing, each sample was added with

Destreak (final concentration: 100 mM) and IPG buffer (final concentration: 0.5%) and then run at 50,000Vhr on 7 cm strips. The second dimension was SDS-PAGE 6%, upon reduction with DTE and alkylation with iodoacetamide of the strips. Resolved proteins were electrotransferred onto Hybond-ECL nitrocellulose membrane with a miniVE Blot Module (GE Healthcare) for 2 h at 300 mA in transfer buffer (25mM trizma base, 40mM glycine, 20% methanol, 0.05% SDS). Membranes were probed for NGL-1. Detection was by enhanced chemiluminescence (ECL) reaction (ECL detection kit, GE Healthcare) and proteins were visualized on autoradiography films (Hyperfilm ECL, GE Healthcare). The lysate (300 μg total protein), without phosphatase inhibitors, was subjected to de-phosphorylation reaction using CIP. Membrane images were acquired with ProXPRESS 2D Proteomic Imaging System and quantitative comparisons of spot intensities were carried out using Progenesis SameSpots (Nonlinear Dynamics, Newcastle upon Tyne, UK).

In uterus electroporation

In uterus electroporation was performed as described previously[41].

Immunocytochemistry for light microscopy

Immunocytochemistry on floating 50 μm brain sections, made with a CM 1850 UV cryostat (Leica), was performed as described previously[41]. Sections were incubated with mouse anti-GFP (clone 3E6; 1:2,000, Invitrogen) and guinea-pig anti-VGLUT1 (1:500, Synaptic System). For teratoma analysis, up to 2×10^6 iPSCs were injected subcutaneously into the dorsal flanks of nude mice. After 3 months, teratoma were explanted, fixed and dissected as described above. Sections were stained with hematoxylin and eosin for further analysis.

Dendritic protrusion analysis

Fluorescent images were acquired using a TCS SP5 laser scanning confocal (Leica) 63× oil-immersion lens as z series of 15-25 images taken at 0.3-μm intervals at 1.024 × 1.024 pixels resolution with 1x zoom. The confocal microscope acquisition parameters were kept the same for all scans for each experiment. Each experiment was repeated at least two, mostly three times and images analyzed in blind using ImageJ (NIH) software. Dendritic protrusion density was measured by counting the number of dendritic protrusions on both, primary and secondary dendrites and expressed as the number of dendritic protrusions per 10 μm dendritic length. Dendritic protrusion length was measured by manually drawing a vertical line from the protrusion's tip to the point where it met the dendritic shaft while head width was measured by drawing a perpendicular line to the length. The proportion of spines in each morphology category was determined for each dendrite. For each experiment, about 300-600 spines from 25-30 dendrites derived from 10-20 neurons were analyzed per condition. In figure legends, *n* refers to the number of neurons quantified. Statistical significance was determined by Student's t-test.

Electrophysiology

Standard patch-clamp whole cell recordings were taken from primary hippocampal neurons transfected at DIV 7 with sh-control or sh-CDKL5#1 and labeled for GFP at DIV 14 as described above. The neurons were continuously perfused with artificial cerebrospinal fluid

(aCSF) of the following composition: 124 mM NaCl, 2 mM KCl, 3 mM KH_2PO_4, 26 mM $NaHCO_3$, 1.3 mM $MgCl_2$, 2.5 mM $CaCl_2$, 10 mM glucose (final pH 7.4). Recording borosilicate glass micropipettes (outside diameter-1.5mm, inside-0.86 mm) were pulled to a resistance of 4-10 MOhms when filled with the following medium: 120 mM KGluconate, 10 mM KCl, 3 mM $MgCl_2$, 10 mM HEPES, 2 mM MgATP, 0.2 mM NaGTP, pH 7.2 (adjusted with KOH), 280mOsm. Miniature excitatory post-synaptic currents (mEPSCs) were observed in the presence of aCSF containing 1 mM tetrodotoxin and 10 mM (-)-bicuculline methiodide, using continuous 60 second epochs of mEPSCs recorded at − 60 mV membrane potential with an Multiclamp 700B amplifier (Molecular Devices, Sunnyvale, CA) with a low pass filter of 2 KHz. Data were digitized at 2-5 KHz with a Digidata 1322A (Molecular Devices) controlled by Clampex 9 software (Molecular Devices) and analyzed off-line with Clampfit 9 software (Molecular Devices), after processing with a band pass of ~2 Hz to 1 KHz using a single pole digital filter. Event selection was visually checked for all data. The statistical analysis was performed using the paired T-test expressing population mean as the mean ± SE.

Recombinant protein purification

hNGL-1 and hNGL-1-S631A were cloned in pTYB1 expression construct, expressed in *E.coli* ER2566 strain and induced with 0.5 mM isopropyl β-D-thiogalactopyranoside (IPTG) at 30°C for 5 h. Following induction, extracts were prepared by resuspending the bacteria in 750 mM NaCl, 20 mM Tris-HCl, pH 8.0, 1 mM EDTA, 0.1% Triton X-100 with protease inhibitors (Sigma) and sonicated. Following centrifugation at 40,000 rpm for 10 min, the lysate was added to chitin-agarose beads (New England Biolabs Inc.). Fusion proteins were cleaved on the column overnight by incubation with lysis buffer containing 50 mM dithiothreitol (DTT). Eluted fractions containing the bulk of NGL-1 were pooled. Recombinant purified NGL-1 and NGL-1-S631A were dialyzed for 16 h at 4°C against the kinase buffer used in the phosphorylation assay.

In vitro phosphorylation assays

HEK293T cells were transfected with 6-Myc-CDKL5 and 6-Myc plasmids. 48 hours after transfection, transfected cells were lyzed in 50 mM Tris-HCl, pH 8.0, 500 mM NaCl, 0.1% NP-40, 1 mM DTT, phenylmethylsulfonyl fluoride and protease and phosphatase inhibitors (Sigma). Equal amounts of protein extracts were pre-cleared for 1 h with 40 μl of 100% mouse IgG-agarose beads at 4°C; 40 μl of 100% agarose conjugate anti-c-Myc (Sigma) was added to the extracts and the mixture incubated for 2 h at 4°C. Immunocomplexes were collected by centrifugation, washed five times and incubated with 1.5 μg of recombinant protein in a kinase buffer in the presence of 7 μCi of [γ-^{33}P] ATP and 25 μM of unlabeled ATP and incubated for 30 min at 30°C. The reaction was stopped by the addition of Laemmli buffer and directly loaded onto a 15% SDS-PAGE; ^{33}P-labeled proteins were detected by autoradiography.

Pull-down

Myc-CDKL5 was first translated *in vitro* using the TNT Quick Coupled Transcription/ Translation System (Promega) and then incubated with Intein-immobilized-chitin-agarose beads or with hNGL-1-Intein-immobilized-chitin agarose beads for 4 h at 4°C.

Immunocomplexes were collected by centrifugation, washed three times with 750 mM NaCl, 20 mM Tris-HCl, pH 8.0, 1 mM EDTA, 0.1% Triton X-100 with protease and phosphatase inhibitors (Sigma), separated on SDS-PAGE and subjected to western blot with anti-Myc and anti-Chitin-Binding-Domain (CBD) antibodies.

Lentivirus and retrovirus production

VSVG-coated particles were packaged in HEK293T cells.

Synaptosome and PSD preparation

The synaptosome fraction was prepared from rat brains as described previously[42]. PSD fractions were prepared from the synaptosome fraction as described previously[43].

Mutation search of *NGL-1* and *NGL-2*

For mutation search the single coding exons of *NGL-1* and *NGL-2* together with their immediately flanking non-coding regions were screened for mutations in a cohort of 51 patients who had been diagnosed with RTT, infantile spasms or a variant of RTT, in whom no *MECP2* or *CDKL5* mutation had been identified. All blood samples were obtained after provision of informed consent. DNAs were amplified by PCR using several primer pairs. Primer sequences are available upon request from V.M.K. PCR products were subjected to denaturing high-performance liquid chromatography or directly sequenced using conventional Sanger sequencing.

Supplementary Material

Refer to Web version on PubMed Central for supplementary material.

Acknowledgments

We gratefully acknowledge T. Bienvenu for providing primary fibroblasts from CDKL5 patients, H. Van Esch and H. Archer for providing DNA samples from patients, S. Freier, A. Walther, A. Grimme, U. Fischer and B. Moser for their excellent technical assistance, and L. Musante for helpful discussions. L. Pecciarini is acknowledged for karyotype analysis of the iPSC lines. This study was supported by Telethon Foundation, Ministry of Health, IIT-SEED project, EuroRETT network to V.B. and the EU-FP7 project GENCODYS (241995) to V.M.K.

References

1. Bienvenu T, Chelly J. Molecular genetics of Rett syndrome: when DNA methylation goes unrecognized. Nat. Rev. Genet. 2006; 7:415–426. [PubMed: 16708070]
2. Chahrour M, Zoghbi HY. The story of Rett syndrome: from clinic to neurobiology. Neuron. 2007; 56:422–437. [PubMed: 17988628]
3. Amir RE, Van den Veyver IB, Wan M, Tran CQ, Francke U, Zoghbi HY. Rett syndrome is caused by mutations in X-linked MECP2, encoding methyl-CpG-binding protein 2. Nat. Genet. 1999; 23:185–188. [PubMed: 10508514]
4. Francke U. Mechanisms of disease: neurogenetics of MeCP2 deficiency. Nat. Clin. Pract. Neurol. 2006; 2:212–221. [PubMed: 16932552]
5. Tao J, Van Esch H, Hagedorn-Greiwe M, Hoffmann K, Moser B, Raynaud M, Sperner J, Fryns JP, Schwinger E, Gécz J, et al. Mutations in the X-linked cyclin-dependent kinase-like 5 (CDKL5/STK9) gene are associated with severe neurodevelopmental retardation. Am. J. Hum. Genet. 2004; 75:1149–1154. [PubMed: 15499549]

6. Weaving LS, Christodoulou J, Williamson SL, Friend KL, McKenzie OL, Archer H, Evans J, Clarke A, Pelka GJ, Tam PP, et al. Mutations of CDKL5 cause a severe neurodevelopmental disorder with infantile spasms and mental retardation. Am. J. Hum. Genet. 2004; 75:1079–1093. [PubMed: 15492925]
7. Archer HL, Evans J, Edwards S, Colley J, Newbury-Ecob R, O'Callaghan F, Huyton M, O'Regan M, Tolmie J, Sampson J, et al. CDKL5 mutations cause infantile spasms, early onset seizures, and severe mental retardation in female patients. J. Med. Genet. 2006; 43:729–734. [PubMed: 16611748]
8. Kalscheuer VM, Tao J, Donnelly A, Hollway G, Schwinger E, Kübart S, Menzel C, Hoeltzenbein M, Tommerup N, Eyre H, et al. Disruption of the serine/threonine kinase 9 gene causes severe X-linked infantile spasms and mental retardation. Am. J. Hum. Genet. 2003; 72:1401–1411. [PubMed: 12736870]
9. Córdova-Fletes C, Rademacher N, Müller I, Mundo-Ayala JN, Morales-Jeanhs EA, García-Ortiz JE, León-Gil A, Rivera H, Domínguez MG, Kalscheuer VM. CDKL5 truncation due to a t(X;2)(p22.1;p25.3) in a girl with X-linked infantile spasm syndrome. Clin. Genet. 2010; 77:92–96. [PubMed: 19807736]
10. Scala E, Ariani F, Mari F, Caselli R, Pescucci C, Longo I, Meloni I, Giachino D, Bruttini M, Hayek G, et al. CDKL5/STK9 is mutated in Rett syndrome variant with infantile spasms. J. Med. Genet. 2005; 42:103–107. [PubMed: 15689447]
11. Rademacher N, Hambrock M, Fischer U, Moser B, Ceulemans B, Lieb W, Boor R, Stefanova I, Gillessen-Kaesbach G, Runge C, et al. Identification of a novel CDKL5 exon and pathogenic mutations in patients with severe mental retardation, early-onset seizures and Rett-like features. Neurogenetics. 2011; 12:165–7. [PubMed: 21318334]
12. Bahi-Buisson N, Nectoux J, Rosas-Vargas H, Milh M, Boddaert N, Girard B, Cances C, Ville D, Afenjar A, Rio M, et al. Key clinical features to identify girls with CDKL5 mutations. Brain. 2008; 131:2647–2661. [PubMed: 18790821]
13. Van Esch H, Jansen A, Bauters M, Froyen G, Fryns JP. Encephalopathy and bilateral cataract in a boy with an interstitial deletion of Xp22 comprising the CDKL5 and NHS genes. Am J Med Genet A. 2007; 143:364–369. [PubMed: 17256798]
14. Mei D, Marini C, Novara F, Bernardina BD, Granata T, Fontana E, Parrini E, Ferrari AR, Murgia A, Zuffardi O, Guerrini R. Xp22.3 genomic deletions involving the CDKL5 gene in girls with early onset epileptic encephalopathy. Epilepsia. 2010; 51:647–54. [PubMed: 19780792]
15. Liang JS, Shimojima K, Takayama R, Natsume J, Shichiji M, Hirasawa K, Imai K, Okanishi T, Mizuno S, Okumura A, et al. CDKL5 alterations lead to early epileptic encephalopathy in both genders. Epilepsia. 2011; 52:1835–1842. [PubMed: 21770923]
16. Bertani I, Rusconi L, Bolognese F, Forlani G, Conca B, De Monte L, Badaracco G, Landsberger N, Kilstrup-Nielsen C. Functional consequences of mutations in CDKL5, an X-linked gene involved in infantile spasms and mental retardation. J. Biol. Chem. 2008; 281:32048–3256.
17. Montini E, Andolfi G, Caruso A, Buchner G, Walpole SM, Mariani M, Consalez G, Trump D, Ballabio A, Franco B. Identification and characterization of a novel serine-threonine kinase gene from the Xp22 region. Genomics. 1988; 51:427–433.
18. Mari F, Azimonti S, Bertani I, Bolognese F, Colombo E, Caselli R, Scala E, Longo I, Grosso S, Pescucci C, et al. CDKL5 belongs to the same molecular pathway of MeCP2 and it is responsible for the early-onset seizure variant of Rett syndrome. Hum. Mol. Genet. 2005; 14:1935–1946. [PubMed: 15917271]
19. Rusconi L, Salvatoni L, Giudici L, Bertani I, Kilstrup-Nielsen C, Broccoli V, Landsberger N. CDKL5 expression is modulated during neuronal development and its subcellular distribution is tightly regulated by the C-terminal tail. J. Biol. Chem. 2008; 283:30101–30111. [PubMed: 18701457]
20. Ricciardi S, Kilstrup-Nielsen C, Bienvenu T, Jacquette A, Landsberger N, Broccoli V. CDKL5 influences RNA splicing activity by its association to the nuclear speckle molecular machinery. Hum. Mol. Genet. 2009; 18:4590–4602. [PubMed: 19740913]
21. Chen Q, Zhu YC, Yu J, Miao S, Zheng J, Xu L, Zhou Y, Li D, Zhang C, Tao J, Xiong ZQ. CDKL5, a protein associated with Rett syndrome, regulates neuronal morphogenesis via Rac1 signaling. J. Neurosci. 2010; 30:12777–12786. [PubMed: 20861382]

22. Rusconi L, Kilstrup-Nielsen C, Landsberger N. Extrasynaptic N-methyl-D-aspartate (NMDA) receptor stimulation induces cytoplasmic translocation of the CDKL5 kinase and its proteasomal degradation. J. Biol Chem. 2011; 286:36550–36558. [PubMed: 21832092]
23. Borg I, Freude K, Kübart S, Hoffmann K, Menzel C, Laccone F, Firth H, Ferguson-Smith MA, Tommerup N, Ropers HH, Sargan D, Kalscheuer V. Disruption of *Netrin G1* by a balanced chromosome translocation in a girl with Rett sindrome. European Journal of Human Genetics. 2005; 13:921–927. [PubMed: 15870826]
24. Woo J, Kwon SK, Kim E. The NGL family of leucine-rich repeat-containing synaptic adhesion molecules. Mol. Cell Neurosci. 2009b; 42:1–10. [PubMed: 19467332]
25. Kim E, Sheng M. The postsynaptic density. Curr Biol. 2009; 19:R723–4. [PubMed: 19906568]
26. Lin JC, Ho WH, Gurney A, Rosenthal A. The netrin-G1 ligand NGL-1 promotes the outgrowth of thalamocortical axons. Nat Neurosci. 2003; 6:1270–1276. [PubMed: 14595443]
27. Kim S, Burette A, Chung HS, Kwon SK, Woo J, Lee HW, Kim K, Kim H, Weinberg RJ, Kim E. NGL family PSD-95-interacting adhesion molecules regulate excitatory synapse formation. Nat. Neurosci. 2006; 9:1294–1301. [PubMed: 16980967]
28. Huttlin EL, Jedrychowski MP, Elias JE, Goswami T, Rad R, Beausoleil SA, Villén J, Haas W, Sowa ME, Gygi SP. A tissue-specific atlas of mouse protein phosphorylation and expression. Cell. 2010; 143:1174–1189. [PubMed: 21183079]
29. Migaud M, Charlesworth P, Dempster M, Webster LC, Watabe AM, Makhinson M, He Y, Ramsay MF, Morris RG, Morrison JH, O'Dell TJ, Grant S,G. Enhanced long-term potentiation and impaired learning in mice with mutant postsynaptic density-95 protein. Nature. 1998; 396:433–439. [PubMed: 9853749]
30. Rosas-Vargas H, Bahi-Buisson N, Philippe C, Nectoux J, Girard B, N'Guyen Morel MA, Gitiaux C, Lazaro L, Odent S, Jonveaux P, Chelly J, Bienvenu T. Impairment of CDKL5 nuclear localisation as a cause for severe infantile encephalopathy. J. Med Genet. 2008; 45:172–178. [PubMed: 17993579]
31. Kim KY, Hysolli E, Park IH. Neuronal maturation defect in induced pluripotent stem cells from patients with Rett syndrome. Proc Natl Acad Sci U S A. 2011; 108:14169–14174. [PubMed: 21807996]
32. Marchetto MC, Carromeu C, Acab A, Yu D, Yeo GW, Mu Y, Chen G, Gage FH, Muotri AR. A model for neural development and treatment of Rett syndrome using human induced pluripotent stem cells. Cell. 2010; 143:527–539. [PubMed: 21074045]
33. Tchieu J, Kuoy E, Chin MH, Trinh H, Patterson M, Sherman SP, Aimiuwu O, Lindgren A, Hakimian S, Zack JA, et al. Female human iPSCs retain an inactive X chromosome. Cell Stem Cell. 2010; 7:329–342. [PubMed: 20727844]
34. Colleoni S, Galli C, Giannelli SG, Armentero MT, Blandini F, Broccoli V, Lazzari G. Long-term culture and differentiation of CNS precursors derived from anterior human neural rosettes following exposure to ventralizing factors. Exp. Cell Res. 2010; 316:1148–1158. [PubMed: 20171210]
35. Bayés A, van de Lagemaat LN, Collins MO, Croning MD, Whittle IR, Choudhary JS, Grant SG. Characterization of the proteome, diseases and evolution of the human postsynaptic density. Nat. Neurosci. 2011; 14:19–21. [PubMed: 21170055]
36. Hering H, Sheng M. Dendritic spines: structure, dynamics and regulation. Nat Rev Neurosci. 2001; 2:880–888. [PubMed: 11733795]
37. Woo J, Kwon SK, Choi S, Kim S, Lee JR, Dunah AW, Sheng M, Kim E. Trans-synaptic adhesion between NGL-3 and LAR regulates the formation of excitatory synapses. Nat. Neurosci. 2009; 12:428–437. [PubMed: 19252495]
38. Han K, Kim E. Synaptic adhesion molecules and PSD-95. Prog Neurobiol. 2008; 84:263–283. [PubMed: 18206289]
39. van Kuilenburg AB, Meijer J, Mul AN, Hennekam RC, Hoovers JM, de Die-Smulders CE, Weber P, Mori AC, Bierau J, Fowler B, et al. Analysis of severely affected patients with dihydropyrimidine dehydrogenase deficiency reveals large intragenic rearrangements of DPYD and a de novo interstitial deletion del(1)(p13.3p21.3). Hum. Genet. 2009; 125:581–90. [PubMed: 19296131]

40. O'Roak BJ, Vives L, Girirajan S, Karakoc E, Krumm N, Coe BP, Levy R, Ko A, Lee C, Smith JD, et al. Sporadic autism exomes reveal a highly interconnected protein network of de novo mutations. Nature. 2012; 485:246–250. [PubMed: 22495309]

41. Ohtsuki T, Horiuchi Y, Koga M, Ishiguro H, Inada T, Iwata N, Ozaki N, Ujike H, Watanabe Y, Someya T, et al. Association of polymorphisms in the haplotype block spanning the alternatively spliced exons of the NTNG1 gene at 1p13.3 with schizophrenia in Japanese populations. Neurosci Lett. 2008; 435:194–197. [PubMed: 18384956]

42. Cohen NA, Brenman JE, Snyder SH, Bredt DS. Binding of the inward rectifier K+ channel Kir 2.3 to PSD-95 is regulated by protein kinase A phosphorylation. Neuron. 1996; 17:759–767. [PubMed: 8893032]

43. Chung HJ, Huang YH, Lau LF, Huganir RL. Regulation of the NMDA receptor complex and trafficking by activity-dependent phosphorylation of the NR2B subunit PDZ ligand. J Neurosci. 2004; 24:10248–10259. [PubMed: 15537897]

44. Essmann CL, Martinez E, Geiger JC, Zimmer M, Traut MH, Stein V, Klein R, Acker-Palmer A. Serine phosphorylation of ephrinB2 regulates trafficking of synaptic AMPA receptors. Nat Neurosci. 2008; 11:1035–1043. [PubMed: 19160501]

45. Kennedy MB, Beale HC, Carlisle HJ, Washburn LR. Integration of biochemical signalling in spines. Nat Rev Neurosci. 2005; 6:423–434. [PubMed: 15928715]

46. Coba MP, Pocklington AJ, Collins MO, Kopanitsa MV, Uren RT, Swamy S, Croning MD, Choudhary JS, Grant SG. Neurotransmitters drive combinatorial multistate postsynaptic density networks. Sci Signal. 2009; 2(68):ra19. [PubMed: 19401593]

Europe PMC Funders Author Manuscripts

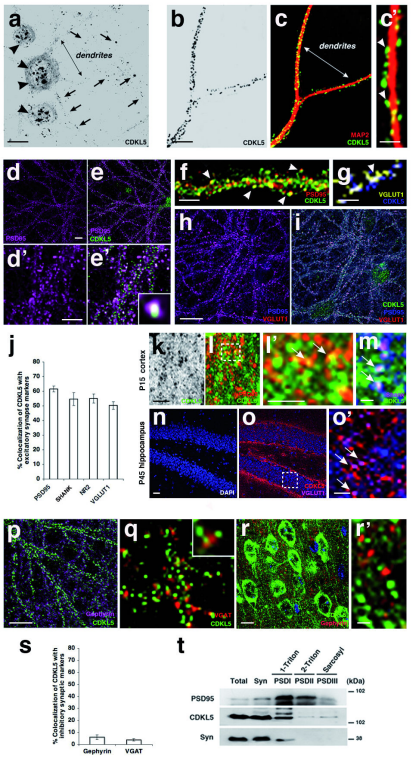

Figure 1.

CDKL5 localizes in dendrites and gathers at excitatory synapses both, *in vitro* and *in vivo*. (**a**) Primary hippocampal neurons immunolabeled at DIV 15 with an antibody against CDKL5. Arrowheads point to intranuclear CDKL5 immunolocalization. Arrows point to CDKL5 immunolabeling in neuronal dendrites. (**b-c'**) Primary hippocampal neurons at DIV 15 co-immunostained for CDKL5 and MAP2. **c'** shows higher magnification of **c**. In **c'**, arrowheads point to CDKL5 dendritic puncta localized to dendritic spines. (**d-f**) Primary hippocampal neurons immunolabeled at DIV 15 with antibodies against CDKL5 and PSD95. **d'** and **e'** show higher magnification of **d** and **e**. Inset in **e'** and arrowheads in **f** show domains of co-localization between CDKL5 and PSD95. (**g**) Immunostaining of hippocampal neurons with CDKL5 and VGLUT1. Arrowhead indicates co-localization of CDKL5 and VGLUT1. (**h**,**i**) Immunostaining of CDKL5 in hippocampal neurons at DIV 15 shows CDKL5 clustering at excitatory synapses co-localizing with PSD95 and apposed to VGLUT1. (**j**) Quantification of the mean percent of co-localization (± s.e.m.) of endogenous CDKL5 with PSD95, Shank, NR2 and VGLUT1. $n = 10$ neurons for each. n derived from three experiments. (**k-o'**) Immunolocalization of CDKL5 in mouse brain also shows CDKL5 clustering at excitatory synapses, as shown by apposition with PSD95 (**l**) or Shank (**m**) in postnatal day (P) 15 mouse cortex and with VGLUT1 in postnatal day (P) 45 mouse hippocampus (**n-o'**). (**l'**) is a higher magnification of the boxed area in **l**. (**o'**) is a higher magnification of the boxed area in **o**. Arrows in **l', m** and **o'** point to a region of co-localization of CDKL5 with either, PSD95, Shank or VGLUT1. (**p-r'**) Immunostaining with CDKL5 and either, gephyrin or VGAT antibodies both, *in vitro* (**p,q**) and *in vivo* (**r,r'**). (**s**) Quantification of the mean percent of co-localization (± s.e.m.) of endogenous CDKL5 with

gephyrin and VGAT. *n* = 10 neurons for each. *n* derived from three experiments. (**t**) CDKL5 is detected in the synaptosomal fraction (Syn) and is enriched in the postsynaptic density fraction I (PSDI). Note that CDKL5 is also detected in postsynaptic density fractions II and III (PSDII and PSDIII). PSD95 and Synaptophysin (Syn) were used as a control. Scale bars: 10 μm (**a**, **b**, **d,** **h**, **k**, **p**, **r**), 5 μm (**d’**, **f**, **l’**, **o’**), 3 μm (**c’**, **g**, **m**), 1 μm (**r’**).

Europe PMC Funders Author Manuscripts

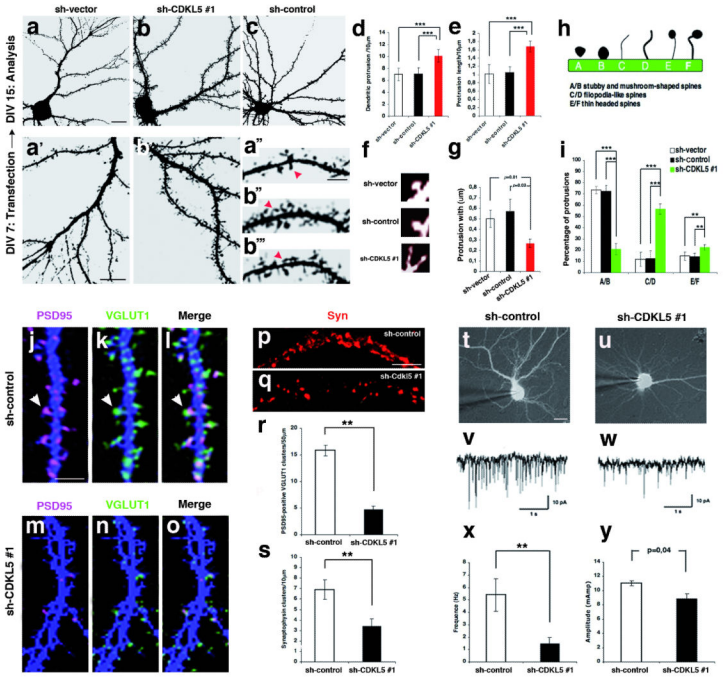

Figure 2.

CDKL5 knock-down alters spine morphology and synaptic activity. **(a-i)** Effects of CDKL5 knock-down on spine morphology. (**a**-**c**) Representative images of primary hippocampal neurons transfected at DIV 7 with sh-vector, sh-control or sh-CDKL5#1 and labeled for GFP at DIV 14. **a'** and **b'** show higher magnifications of (**a**) and (**b**). **a''**, **b''** and **b'''** represent higher magnifications of (**a**) and (**b**) and show the spine phenotype in single GFP-positive dendrites expressing either, sh-vector or sh-CDKL5#1. In **a''**, **b''** and **b'''**, arrowheads point to dendritic protrusions. (**d**,**e**) Quantification of dendritic protrusion density (**d**) and length (**e**) of sh-vector, sh-control and sh-CDKL5#1 transfected neurons. Bar graphs show mean ± s.e.m. *n* = 15 neurons for sh-vector, *n* = 18 neurons for sh-control and sh-CDKL5#1 (***p<0.001, t test). *n* derived from four independent experiments. (**f**,**g**) CDKL5 down-regulation decreases spine width. Bar graphs show mean ± s.e.m. *n* = 15 neurons for sh-vector, *n* = 18 neurons for sh-control and sh-CDKL5#1 each. *n* derived from four independent experiments. (**h**) Schematic representation of dendritic protrusion morphology categories. (**i**) Quantification of the mean percent of spines in each morphology category in neurons expressing sh-vector, sh-control or sh-CDKL5 #1. Bar graphs show mean ± s.e.m. *n* = 15 neurons for sh-vector, *n* = 18 neurons for sh-control and sh-CDKL5#1 each (***p<0.001, **p<0.01, t test). *n* derived from four independent experiments. (**j**-**s**) CDKL5 knock-down affects excitatory synapse number. Primary hippocampal neurons were transfected at DIV 7 with sh-control or sh-CDKL5#1 and immunostained at DIV 14 with the indicated antibodies. **l** and **o** represent merged images. Arrowheads in **j**, **k** and **l** indicate co-localization of PSD95 with VGLUT1 at dendritic spines. Bar graphs in **r** and **s** show mean ± s.e.m. *n* = 16 neurons for sh-control and sh-CDKL5#1 each (**p<0.01, t test). *n* derived from three independent experiments. (**t**-**y**) CDKL5 knock-down in DIV 15 cultured neurons reduced the frequency (**x**) and the amplitude (**y**) of mEPSCs. *n* = 9 neurons for sh-control

Europe PMC Funders Author Manuscripts

and *n* = 13 neurons for sh-CDKL5#1 (**p<0.01, t test). *n* derives from two independent experiments. Scale bar: 10 μm (**a**, **a'**, **j**, **p**, **t**), 5 μm (**a''**).

Europe PMC Funders Author Manuscripts

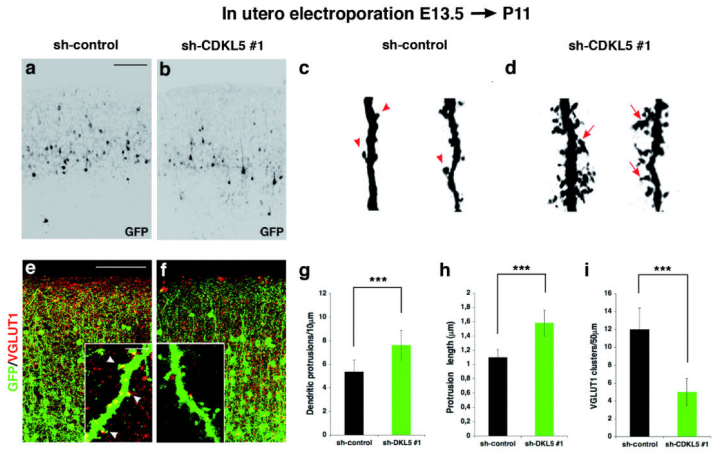

Figure 3.

CDKL5 knock-down impairs spine structure and excitatory synapse density *in vivo*. (**a**,**b**) Representative confocal images of coronal slices of postnatal day (P) 11 mouse brains transfected with sh-control or sh-CDKL5#1 by *in utero* electroporation at E13.5. Many transfected GFP-positive cells were detected in each transfection condition. (**c**,**d**) Representative images of single dendrites of GFP-positive cortex pyramidal neurons expressing sh-control or sh-CDKL5#1. Arrows and arrowheads point to morphological normal and aberrant spines, respectively. (**e**,**f**) Representative confocal images of cortex pyramidal neurons transfected with either sh-control or sh-CDKL5#1 and immunostained for GFP and VGLUT1. Arrowheads in (**e**) show co-localization of CDKL5 and VGLUT1 at dendritic spines. (**g**,**h**) Quantitative analysis of dendritic protrusion density and length of GFP-positive cortex pyramidal neurons. Bar graphs show mean ± s.e.m. $n = 15$ neurons for each condition (***p<0.001, t test). n derived from three independent experiments. (**i**) Quantitative analysis of VGLUT1 clusters in GFP-positive cortex pyramidal neurons. Bar graphs show mean ± s.e.m. $n = 9$ neurons for each condition (***p<0.001, t test). n derived from three independent experiments. Scale bar: 100 µm (**a**, **e)**.

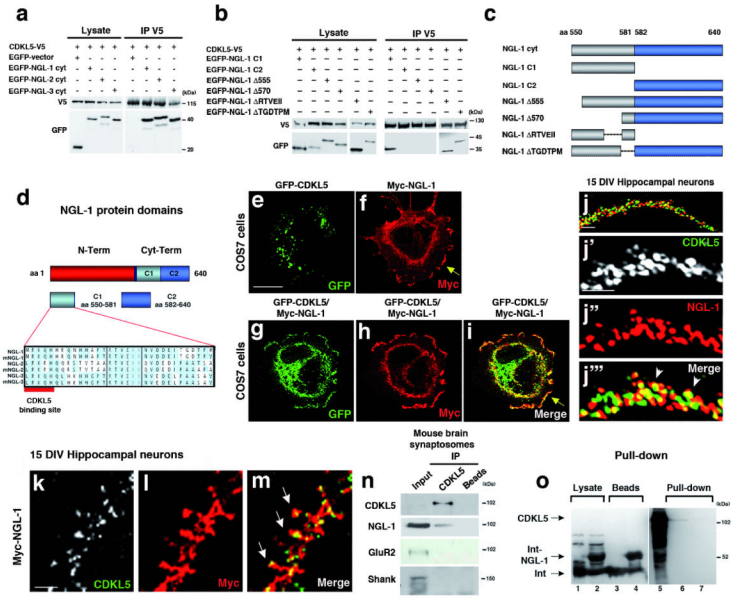

Figure 4.

CDKL5 and NGL-1 interact *in vitro* and *in vivo.* (**a**) HEK293T cells were co-transfected with CDKL5-V5 and EGFP NGL-1, -2, -3 constructs representing their intracellular cytoplasmic region. Cell lysates were immunoprecipitated with anti-V5 antibody. Western blots were probed with anti-V5 or anti-GFP-HRP antibody. (**b)** HEK293T cells were co-transfected with CDKL5-V5 and various EGFP-NGL-1 cyt deletion constructs. Cell lysates were immunoprecipitated with anti-V5 antibody. Western blots were probed with anti-V5 or anti-GFP-HRP antibody. **(c**) Schematic representation of deletion clones used for determining the CDKL5 binding site in the intracellular C-terminal domain of NGL-1. (**d**) Schematic representation of NGL-1 protein together with its intracellular C-terminal domain (Cyt-Term) and CDKL5 binding site. (**e-i**) Co-clustering assay in COS-7 cells expressing GFP-CDKL5 (**e**), Myc-NGL-1 (**f**) and GFP-CDKL5 in combination with Myc-NGL-1 (**g-i**). (**i**) Merged image. Arrow in **i** shows redistribution of GFP-CDKL5 on the plasma membrane upon co-transfection with NGL-1. (**j-j'''**) Primary hippocampal neurons labeled at DIV 15 for CDKL5 and NGL-1. Arrowheads in **j'''** show colocalization of CDKL5 with NGL-1 (**k-m**) Primary hippocampal neurons transfected with Myc-NGL-1 at DIV 7 and 7 days later labeled for CDKL5 and Myc-NGL-1 to detect endogenous CDKL5 and recombinant Myc-NGL-1 protein. In **m,** arrows point to a region of co-localization between CDKL5 and NGL-1 at dendritic spines. (**n**) Interaction of endogenous NGL-1 with CDKL5 by co-immunoprecipitation from synaptosome lysates of postnatal day (P) 4 mouse brain. Anti-GluR2 and anti-Shank antibodystainings served as negative control. (**o**) Intein fusion protein of NGL-1 (amino acids 550-640) pulls down CDKL5. Lanes 1 and 2: cellular lysate of IPTG induced samples; lanes 3 and 4: Intein or Intein-NGL-1-immobilized agarose beads; lane 5: CDKL5 input; lanes 6 and 7: CDKL5 pull-down induced by Intein-NGL-1 or Intein alone. Scale bar: 10 μm (**e**), 5 μm (**j**, **j' k**).

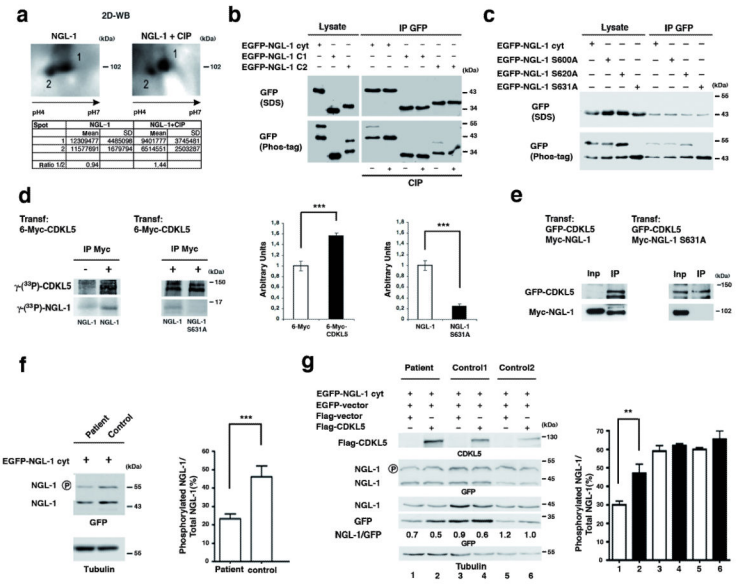

Figure 5.

CDKL5 mediates phosphorylation in NGL-1 at Ser-631. (**a**) Total brain extracts were left untreated (left panel) or were treated with alkaline phosphatase (CIP) (right panel), subjected to 2-D gel electrophoresis and analyzed by immunoblotting with anti-NGL-1 antibody. In **a**, the table reports the results of the densitometric scanning quantification of the spots 1 and 2 and the ratio (½) of both, in control and CIP treated samples. (**b**) Immunoprecipitations performed with anti-GFP antibody of HEK293T cells lysates transfected with the indicated plasmids and treated with CIP (+) or left untreated (-). Proteins were resolved in normal SDS-PAGE gels (upper panel) and in phosphate-affinity PAGE gels (lower panel). (**c**) HEK293T cells were transfected with EGFP-NGL-1 cyt, EGFP-NGL-1 S600A, EGFP-NGL-1 S620A or EGFP-NGL-1 S631A constructs. Immunoprecipitations were performed with anti-GFP antibody. Proteins were resolved in a normal SDS gel (upper panel) and a Phos-Tag gel (lower panel). (**d**) In vitro kinase assay performed of HEK293T cell lysates transfected with the indicated plasmids. The mean relative NGL-1 and NGL-1 S631A phosphorylation is illustrated in a bar graph (***p<0.001, t test). (**e**) Total cell lysates of HEK293T cells transfected with the indicated plasmids were subjected to immunoprecipitations with monoclonal anti-GFP and anti-Myc antibodies. (**f**) Control and CDKL5 negative patient fibroblast cells were transfected with EGFP-NGL-1 cyt. Total cell lysates were resolved in a Phos-Tag SDS gel and probed with anti-GFP-HRP antibody. Anti-tubulin antibody staining served as loading control. The relative NGL-1 phosphorylation is presented as means +/− SD of four independent experiments compared to the total amount of NGL-1 (***p<0.001, t test). (**g**) Total cell lysates of both, control and CDKL5 negative patient fibroblast cells were transfected with the indicated plasmids and resolved in a normal SDS gel or in a Phos-Tag SDS gel. GFP protein levels were used to monitor transfection efficiency as indicated in NGL-1/GFP ratios (given in arbitrary units). The relative NGL-1 phosphorylation is presented as means +/− SD of three independent experiments compared to the total amount of NGL-1 (**p<0.01, t test).

Europe PMC Funders Author Manuscripts

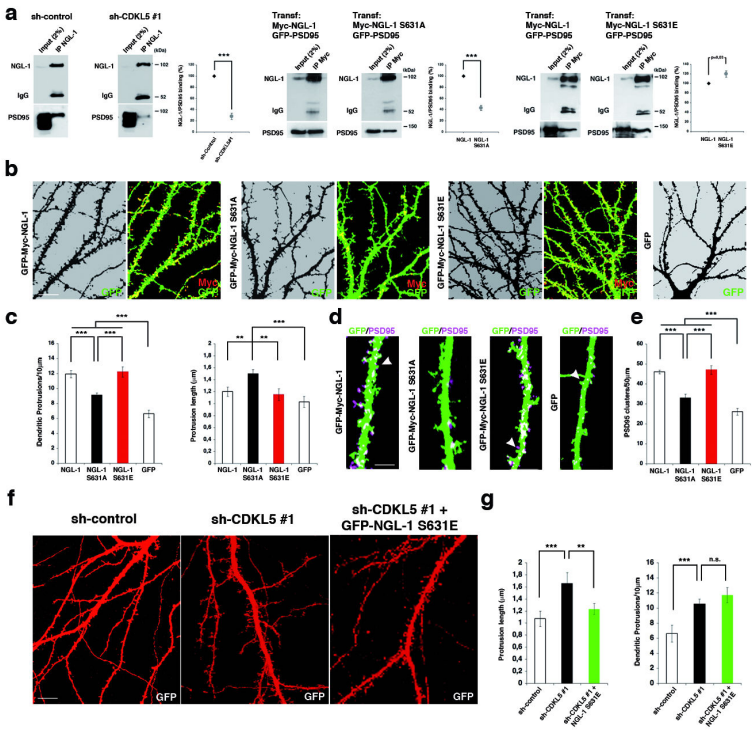

Figure 6.

CDKL5-dependent phosphorylation of NGL-1 is necessary for NGL-1/PSD95 binding and correct spine morphogenesis. (**a**) CDKL5 knock-down reduces NGL-1/PSD95 binding in primary cortical neurons (left panel). Lysates of primary cortical neurons (DIV 14) infected with either sh-control or sh-CDKL5#1, were immunoprecipitated with antibodies against NGL-1 and immunoblotted with NGL-1 and PSD95 antibodies. CDKL5-dependent phosphorylation of NGL-1 on S631 sustains NGL-1 binding to PSD95 (middle panel). Lysates of HEK293T cells double-transfected with GFP-PSD95 plus Myc-NGL-1 or Myc-NGL-1-S631A were immunoprecipitated using an antibody against Myc and immunoblotted with Myc and PSD95 antibodies. Lysates of HEK293T cells double-transfected with GFP-PSD95 plus Myc-NGL-1 or Myc-NGL-1-S631E were immunoprecipitated using an antibody against Myc and immunoblotted with Myc and PSD95 antibodies (right panel). (**b**,**c**) Effect of overexpression of wild-type NGL-1, NGL-1-S631A and NGL-1 S631E on dendritic protrusion density and morphology. Primary hippocampal neurons were transfected with the indicated plasmids at DIV 7 and 7 days later were stained for GFP and Myc. In **c**, bar graphs show mean ± s.e.m. *n* = 12 neurons for each (***p<0.001, **p<0.01, t test). *n* derived from three independent experiments. (**d**,**e**) Primary hippocampal neurons were transfected with the indicated plasmids at DIV 7 and were stained for GFP and PSD95 7 days after transfection. In **d**, arrowheads point to dendritic spines. In **e**, bar graphs show mean ± s.e.m. *n* = 10 neurons for each (***p<0.001, t test). *n* derived from three independent experiments. (**f**) NGL-1 S631E partially rescues the phenotype of CDKL5 knock-down. Representative images of primary hippocampal neurons transfected at DIV 7 with the indicated plasmids and labeled for GFP at DIV 14. (**g**) Quantification of dendritic protrusion density and length of sh-control, sh-CDKL5 #1 and sh-CDKL5 #1 plus GFP-

Europe PMC Funders Author Manuscripts

NGL-1 S631E transfected neurons. Bar graphs show mean ± s.e.m. *n* = 12 neurons for each (***p<0.001, **p<0.01, t test). *n* derives from three independent experiments. Scale bar: 10 μm (**b, f**), 5 μm (**d**).

Europe PMC Funders Author Manuscripts

Europe PMC Funders Author Manuscripts

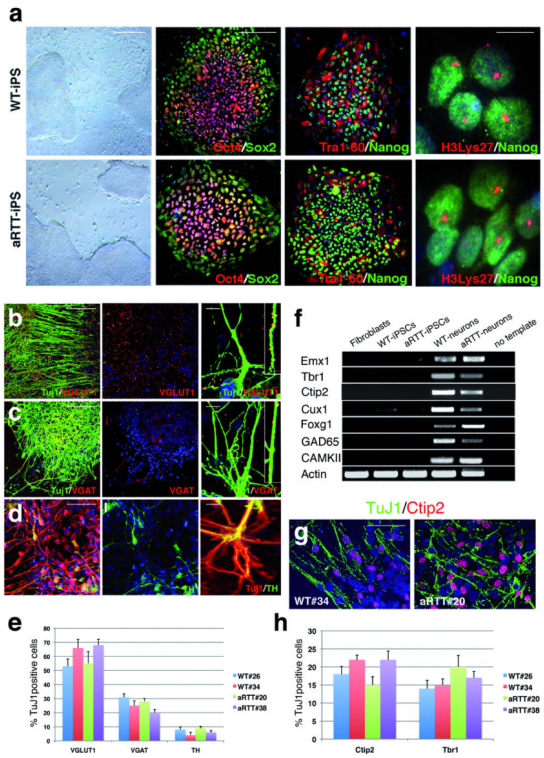

Figure 7.

Assessment of pluripotency-associated markers in iPSCs and forebrain identity of iPSC-derived neurons. (**a**) Bright field images of iPSC colonies in the growing phase. iPSCs express pluripotency markers such as OCT4, SOX2, NANOG and TRA-1-60 and display a H3K27^{+} inactivated X-chromosome. (**b-d**) Cultured iPSC-derived neurons were immunolabeled with Tuj1 antibody in combination with either, VGLUT1, VGAT or TH antibodies. (**e**) Quantification of the mean percent of either VGLUT1, VGAT or TH-positive Tuj1 cells for the neuronal progenies differentiated from 4 different iPSC lines. Bar graphs show mean ± s.e.m. *n* = 390 neurons (*n* derived from three independent experiments per line). (**f**) RT-PCR expression analysis of specific brain area genes. iPSC-derived neurons expressed markers of forebrain identity as *Emx1*, *Tbr1*, *Ctip2*, *Cux1, CAMKII* and *Foxg1*. (**g**) iPCS-derived TuJ1+ neurons express the cortical layers-5 molecular marker Ctip2. (**h**) Quantification of the mean percent of Ctip2 and Tbr1 expression in TuJ1+ neurons. Bar graphs show mean ± s.e.m. *n* = 360 neurons (*n* derived from three independent experiments per line). Scale bar: 100 μm (**a**, **b, c, d**), 50 μm (**d**, **g**), 10 μm (**a**, **b**, **c**, **d**).

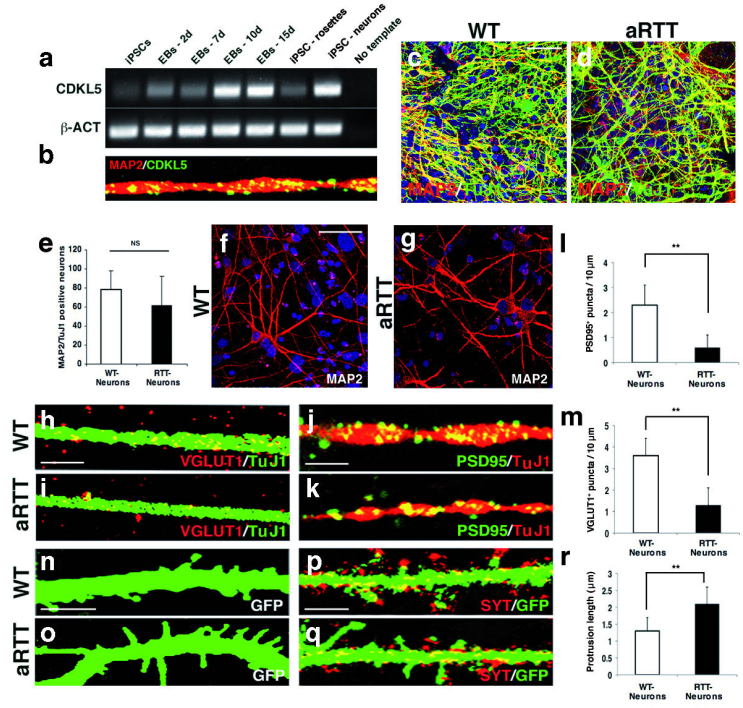

Figure 8.

Patient specific iPSC-derived neurons exhibit normal differentiation rate, but aberrant spine structures. (**a**) *CDKL5* transcripts increased in embryoid bodies and during neuronal differentiation. (**b**) CDKL5 immunofluorescence showing its localization enriched at the synapses of iPSC-derived neurons. (**c**,**d**) Low magnification view of both, affected and healthy iPSC-derived neuronal cultures immunodecorated for MAP2 and TuJ1. (**e**) Neuronal differentiation rate is not altered in aRTT. *n* = 250 neurons (*n* derived from five independent experiments per line), NS = Not significant. (**f**,**g**) Representative images of 62 days old WT and aRTT iPSC-derived neurons immunostained for MAP2. (**h**-**k**) High magnification images on dendritic tracts of WT and aRTT iPSC-derived neurons processed for VGLUT1/TuJ1 and PSD95/TuJ1 antibody staining. (**l**,**m**) Quantitative analysis reveals a reduced number of both, VGLUT1 (**h**,**i**) and PSD95 puncta (**j**,**k**) in the aRTT compared to WT neurons. Bar graphs show mean ± s.e.m. *n* = 580 spines. (*n* derived from five independent experiments per line) (**p<0.01, t test). (**n**,**o**) GFP visualization permits to identify aberrant spines with very long and thin appearance in aRTT neurons. (**p**,**q**) Aberrant spines in aRTT neurons lack an evident presynaptic terminal as showed by immunofluorescence for synaptophysin (SYT). (**r**) Quantification of the mean length of dendritic spines in WT and aRTT neurons. Bar graphs show mean ± s.e.m. *n* = 550 spines (*n* derived from five independent experiments per line). (**p<0.01, t test). Scale bar: 50 µm (**c**, **f**), 20 µm (**j**), µm (**h**), 5 µm (**n**, **p**).

Europe PMC Funders Author Manuscripts